2008 American Control Conference
Westin Seattle Hotel, Seattle, Washington, USA
June 11-13, 2008

A Novel Application of An Extended State Observer for High Performance Control of NASA's HSS Flywheel and Fault Detection

B. X. S. Alexander, Richard Rarick, Lili Dong

Abstract—**A novel application, employing the strategy of Active Disturbance Rejection Control and an Extended State Observer, is proposed to control the rotor shaft position of NASA's High Speed Shaft (HSS) Flywheel using active magnetic bearings. The robustness of the control is demonstrated in a frequency domain analysis and in simulations to be a major improvement of controls recently studied at NASA.**

Keywords: **Active Disturbance Rejection Control, Extended State Observer, Flywheel Energy Storage.**

I. INTRODUCTION

For long-duration space applications, such as the space station, batteries are required to supply power during the periods when the solar arrays are in eclipse. The expensive maintenance and replacement requirements of batteries have prompted investigation into flywheel energy storage devices as an alternative to current battery technology. The flywheel rotors achieve high energy densities by being driven to rotational speeds in excess of 60,000 rpm, necessitating the use of magnetic bearings [1][2].

Current research at the NASA Glenn Research Center (GRC) is focused on the High Speed Shaft (HSS), a flywheel system capable of reaching speeds up to 100,000 rpm. The suspension of the flywheel rotor is achieved by means of opposing sets of electromagnets in the radial direction, between which the rotor is positioned (Figure 1, [4]). The position of the rotor in the air gap can be controlled via magnetic forces which are regulated by adjusting the magnet coil voltage. The magnetic forces exert attractive forces on the rotor shaft which is coated with ferromagnetic material. Because of the attractive nature of the magnetic forces, magnetic bearings are inherently unstable and require closed-loop control.

Numerous advanced controller design approaches have been proposed for this type of application. Hubbard [5] used linear-quadratic design in his pendulous supported flywheel. Stanway [6] used eigenstructure assignment for the control of suspension systems for rotating machinery within a magnetic field. Sinha [7] considered sliding mode control of a rigid motor using magnetic bearings. Salm [8] demonstrated modal control of a flexible rotor. Matsumura [9] used an integral type servo-controlled design via solution of a linear quadratic regulator problem for a horizontal rotor-magnetic-bearing system. And Hung [10] considered magnetic bearing control using fuzzy logic.

These proposed controllers are often of such a complexity that the tuning process is rendered quite difficult. The PID controller, however, because of its ease of tuning, has been the only controller used at GRC for flywheel levitation [3]. Recently, a PD controller, supplemented with an observer for velocity feedback, was studied and shown to reduce noise and control effort [4]. However, the observer required additional tuning, and the robustness of the observer against variations in plant parameters was poor. The combined control system was also poor at rejecting a constant force disturbance.

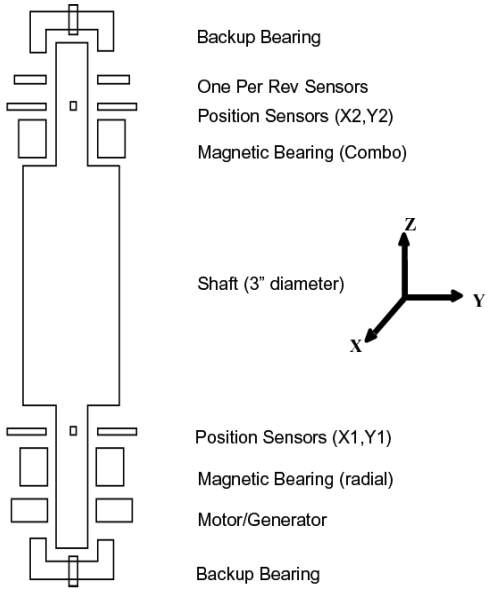

Figure 1. Schematic: HSS Flywheel module components

Based on the plant model developed in [4], a novel application, employing the strategy of Active Disturbance Rejection Control (ADRC) and an Extended State Observer (ESO) [11][12][14][19], is proposed to control the rotor shaft position. Using only one tuning parameter, the ESO requires minimal tuning effort. A frequency-domain analysis shows that the combination of PD/ESO feedback results in

The authors are with the Department of Electrical and Computer Engineering at Cleveland State University, Cleveland, OH 44115, USA.

robust performance against variations in plant parameters. It is also capable of rejecting constant force disturbances.

The plant model of the magnetic bearing is introduced in Section II. The ESO is developed in Section III and analyzed in IV. Time-domain simulation results are shown to validate the frequency-domain analysis in Section V. In Section VI, the controller is applied to a three-degrees of freedom rotor vibration model, which is nonlinear and time-varying.

II. Magnetic Bearing Model

As illustrated in Figure 1, two radial magnetic bearing are used in NASA's HSS module, one attached to each end of the rotor. We will only concern ourselves with a simplified, single degree-of-freedom system in the controller design. In such a case, the mechanical system can be modeled as a single-input, single output (SISO) plant, where the output is the position and the input the actuation force of the magnets. The results can be extended in a straightforward manner to a multiple degrees-of- freedom system, which is briefly discussed in Section VI.

The position transfer function of the rotor can be obtained from the physical model of the electromechanical components. If the rotor is assumed to be rigid and damping assumed to be negligible, the plant can be represented by a mass-spring system. The corresponding force diagram is shown in Figure 2 [4].

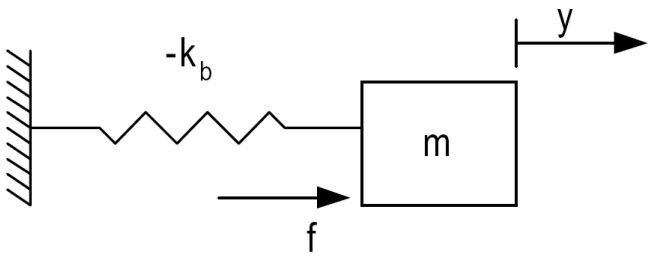

Figure 2: Force diagram for rotor position model

The position of the rotor, x, can be controlled by the actuator force, F, which is generated by the electromagnets. The functional relationship between magnetic coil current and output magnetic force is usually known with a high degree of accuracy. Following the analysis in [4], the magnetic force is the control input signal. In actual implementation, the magnetic force can easily be converted into a control current or voltage signal. From Figure 2, the differential equation for the rotor dynamics is given by,

$$m\ddot{x} - K_b x = F \,, \tag{2.1}$$

where m is the mass of the rotor, and K_b is the value of the experimentally determined stiffness constant. By taking the Laplace transform of (2.1), one can obtain the open-loop position transfer function,

$$\frac{X(s)}{F(s)} = \frac{1}{ms^2 - K_b} \tag{2.2}$$

which has poles at $\pm\sqrt{K_b/m}$. The presence of a pole in the right half-plane renders the system unstable, so closed-loop control must be applied in order to stabilize it. The physical significance of the closed-loop control is that the resulting system has an adjustable, positive stiffness and damping factor.

III. Control Strategy

As emphasized repeatedly in [4], the observer gains are difficult to tune because of their sensitivity to variations in plant parameters. During the operation of the flywheel, the actual parameter values of the plant may change because of variations in rotor imbalance, friction, coil resistance, and so on. Classical observer design, which relies on the exact model of the plant, is very sensitive to changes in plant parameters, and this, in turn, may affect the stability of the observer.

Recently, an innovative observer design, the Extended State Observer (ESO) has been developed [11][12][14], which relaxes the requirement of the exact knowledge of the plant. This greatly reduces the sensitivity of the observer to the values of the plant parameters. The ESO estimates real-time variations in the plant parameters and compensates for them online. In the seminal papers by Miklosovic and Radke [15] [16], the PD/ESO controller was extended to a wide class of systems.

The following mathematical development applies to any second-order plant, whether linear or non-linear, and can be generalized to systems of arbitrary-order [17].

A more general form of the second-order plant in Equation (2.1) is given by

$$\ddot{x} = f(x, \dot{x}, t) + bu \,, \tag{3.1}$$

where the position, x, now denotes the output of the plant, and u denotes the control input of the plant, the force F. The control input gain, b, can be identified as $b = 1/m$ from equation (2.1). The function f represents the remaining terms in the differential equation. This function is referred to as a *generalized disturbance* [12]. If the generalized disturbance can somehow be cancelled, the plant in (3.1) would reduce to a simple, double-integrator plant. The goal of ESO design is to estimate the generalized disturbance, and to compensate for it in real-time, so that the system is forced to behave like a double-integrator plant.

The key to ESO design is to interpret the generalized disturbance f as an additional state of the dynamical system. For a second-order system, the number of states would now

increase from two to three. The states variables for the ESO are chosen as follows:

$$\begin{aligned} x_1 &= x \\ x_2 &= \dot{x} \\ x_3 &= f \end{aligned} \tag{3.2}$$

The inclusion of f as an additional third state is what motivated the name *Extended State* [11]. The extended state representation of the system dynamics can be derived directly from (3.1),

$$\begin{aligned} \dot{x}_1 &= x_2 \\ \dot{x}_2 &= x_3 + bu \\ \dot{x}_3 &= h \\ y &= x_1 \end{aligned} \tag{3.3}$$

where h is the time derivative of f. The corresponding state space model is

$$\begin{aligned} \dot{\mathbf{x}} &= \mathbf{A}\mathbf{x} + \mathbf{B}u + \mathbf{E}h \\ y &= \mathbf{C}\mathbf{x} \end{aligned} \tag{3.4}$$

where the matrixes are

$$\mathbf{A} = \begin{bmatrix} 0 & 1 & 0 \\ 0 & 0 & 1 \\ 0 & 0 & 0 \end{bmatrix}, \quad \mathbf{B} = \begin{bmatrix} 0 \\ b_0 \\ 0 \end{bmatrix}, \quad \mathbf{C} = \begin{bmatrix} 1 \\ 0 \\ 0 \end{bmatrix}^T, \quad \mathbf{E} = \begin{bmatrix} 0 \\ 0 \\ 1 \end{bmatrix} \tag{3.5}$$

Based on (3.4), the ESO is constructed as follows [12]:

$$\begin{aligned} \dot{\hat{\mathbf{x}}} &= \mathbf{A}\hat{\mathbf{x}} + \mathbf{B}u + \mathbf{L}\left(y - \mathbf{C}\hat{\mathbf{x}}\right) \\ &= \left(\mathbf{A} - \mathbf{L}\mathbf{C}\right)\hat{\mathbf{x}} + \mathbf{B}u + \mathbf{L}\mathbf{C}\mathbf{x} \end{aligned} \tag{3.6}$$

The states of this observer correspond to the estimated values of the quantities,

$$\begin{aligned} \hat{x}_1 &\approx x \\ \hat{x}_2 &\approx \dot{x} \\ \hat{x}_3 &\approx f \end{aligned} \tag{3.7}$$

which yields the desired estimate for the generalized disturbance $x_3 = f$. The observer gain vector L can be denoted as

$$\mathbf{L} = \left[\beta_1,\ \beta_2\ ,\beta_3\right]^T \tag{3.8}$$

and the observer gains can be computed following the parameterization technique introduced in [12]:

$$\beta_1 = 3\omega_o, \qquad \beta_2 = 3\omega_o^2, \qquad \beta_3 = \omega_o^3 \tag{3.9}$$

When substituted into the matrices into (3.8) and (3.6), the result is

$$\mathbf{L} = \begin{bmatrix} 3\omega_O \\ 3\omega_O^2 \\ \omega_O^3 \end{bmatrix} \quad \text{and} \quad \mathbf{A} - \mathbf{L}\mathbf{C} = \begin{bmatrix} -3\omega_O & 1 & 0 \\ -3\omega_O^2 & 0 & 1 \\ -\omega_O^3 & 0 & 0 \end{bmatrix} \tag{3.10}$$

We note that the **A** and **B** matrices are constant and do not depend on a detailed knowledge of the plant. This feature enables one to choose the observer gains without such knowledge and is one of the reasons why the ESO is less sensitive to variations in plant parameters than classical observers.

When the extended state observer is properly designed, it will compensate for the generalized disturbance. Assuming accurate estimation of f and approximate knowledge of b, that is,

$$\begin{aligned} f &\approx \hat{x}_3 \\ b &\approx b_0 \end{aligned} \tag{3.11}$$

the compensated plant will be shown below to be a double-integral plant, which is then easily controlled using a PD controller. Using ADRC strategy, the control law is given by

$$u = \left(u_0 - \hat{x}_3\right)/b_0\,, \tag{3.12}$$

where the term $-\hat{x}_3$ compensates for the generalized disturbance f, and the term u_0 is the PD control law given by

$$u_0 = k_p\left(r - \hat{x}_1\right) - k_d\hat{x}_2\ . \tag{3.13}$$

Here r is the set point, and k_p and k_d are the PD controller gains. Substituting (3.12) into (3.1) and assuming the conditions in (3.11), Equation (3.1) is approximated by a double-integrator plant controlled by u_0:

$$\ddot{x} \approx u_0$$

or,

$$\ddot{x} \approx k_p\left(r - x\right) - k_d\dot{x} \tag{3.15}$$

The combined control law for the PD/ESO is,

$$u = \frac{1}{b_0}\left[k_p\left(r - \hat{x}_1\right) - k_d\hat{x}_2 - \hat{x}_3\right] \tag{3.16}$$

The tuning of the PD controller can be simplified as follows. The Laplace transform of (3.15) gives the closed-loop transfer function

$$\frac{X(s)}{R(s)} = \frac{k_p}{s^2 + k_d s + k_p} \tag{3.17}$$

where $X(s)$ and $R(s)$ are the Laplace transforms of x and r, resp. Using the transfer function of a standard second-order system with critical damping, namely,

$$\frac{X(s)}{R(s)} = \frac{\omega_c^2}{\left(s + \omega_c\right)^2}\,, \tag{3.18}$$

Equations (3.17) and (3.18) can be set equal to obtain the PD gains in terms of the parameter ω_c:

$$k_p = \omega_c^2 \quad \text{and} \quad k_d = 2\omega_c . \qquad (3.19)$$

IV. Frequency Analysis of the PD/ESO

The closed-loop stability and robustness of a control system is a main concern for new control algorithms. Because of the linear nature of the plant, the controller (PD), and observer (ESO), stability can be assessed using frequency-response methods. In particular, the open-loop Nyquist and Bode diagrams are used in this case.

Figure 3 shows the Nyquist plot of the open-loop transfer function of the plant with the stiffness and mass chosen as $K_b = 0.25$, $m = 1$, and the controller parameters set at $\omega_0 = \omega_c = 105$ and $b_0 = 1/m$. As seen in (2.2), the open-loop system has one RHP pole, so the counter-clockwise encirclement of –1 guarantees a stable closed-loop system under negative feedback. Therefore, a Bode analysis is valid.

The Bode gain plot in Figure 4 intersects the 0dB line at a crossover frequency of 105 rad/s. The gain margin is relatively large near the crossover frequency. The Bode phase plot reaches its maximum at this frequency, exhibiting a locally symmetric peak that gives a phase margin of 31.9 degrees.

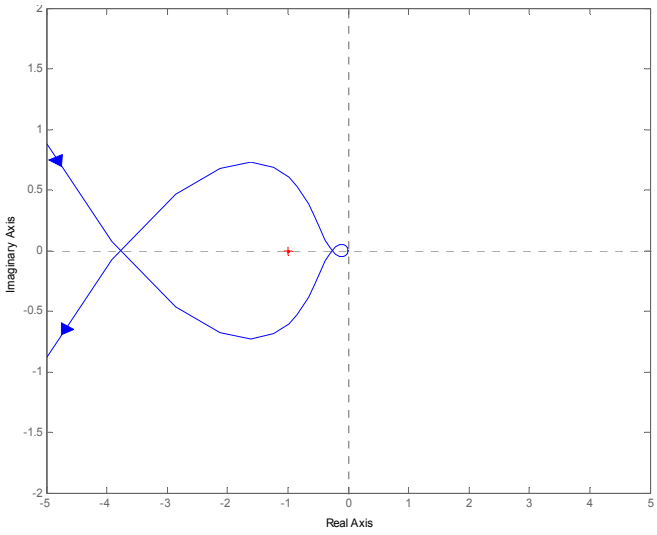

Figure 3: Nyquist plot of LADRC open-loop gain

Another concern, which was raised specifically in [4], is the robustness of the closed-loop system against variations in plant parameters. In particular, the stiffness constant is prone to vary [13] because of physical changes in the rotor, as well as changes in coil resistance, due to changes in temperature. The robustness against variations in the stiffness constant is assessed using Bode diagrams.

The different plots in Figure 4 show the effect of changes in the stiffness constant as large as 17 times its original value, while keeping all other plant and controller parameters constant. The changes in K_b have only a minimal effect on the Bode plots. In particular, the shape remains identical in the vicinity of the crossover frequency. This fact demonstrates the robustness of the PD/ESO control loop in the presence of variations in plant parameters.

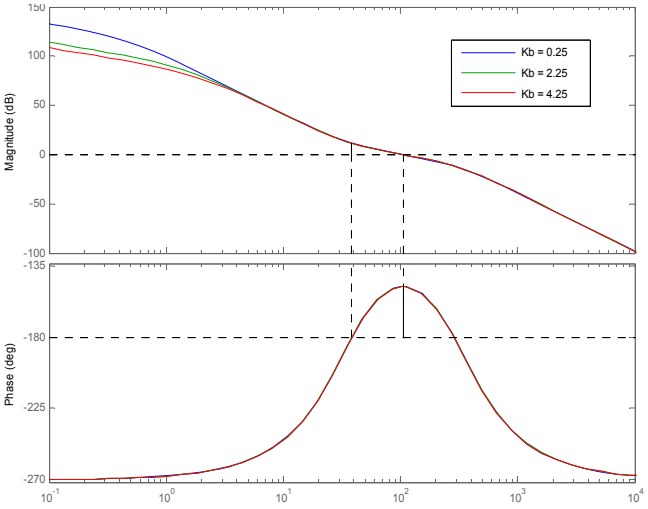

Figure 4: Effect of variation in stiffness constant K_b

V. Simulation Results – One Degree of Freedom

The objective of magnetic bearing control is to maintain the rotor at a steady-state position of $x = 1\times10^{-3}$ m. The rotor is assumed to be levitated at the steady state position. Adequate position sensor noise is added in all simulations.

The simulation results presented in this section serve two purposes. The first simulation corroborates the frequency response analysis. It also shows that the PD/ESO control is more robust against variations in plant parameters than the classical PD/observer. The second simulation shows that the PD/ESO is capable of rejecting a constant force disturbance.

Under ideal circumstances, when the plant parameters remain constant during the operation of the flywheel, that is, if the stiffness remains constant, the PD/ESO and the PD/observer lead to very similar control performance. However, in more realistic circumstances, the actual value of the stiffness constant may vary over a large range during operation.

In the first simulation, which is shown in Figure 5, the value of the stiffness constant was changed from its original value of K_b = 0.25 N/m to K_b = 4 N/m, while all controller parameters were left unchanged as in the preceding

discussion. Figure 6 shows the effect when a force disturbance, Fs = -0.001N is applied at 4 seconds. With the PD/ESO, the rotor recovers within 1 second to its steady-state position.

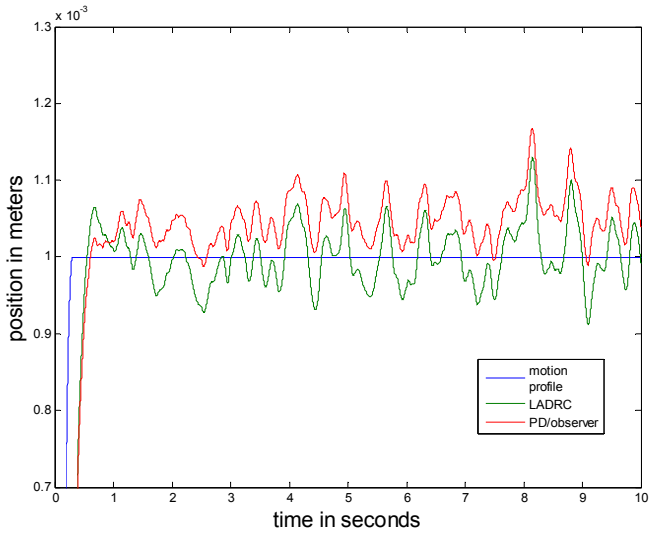

Figure 5: Rotor position control performance comparison (K_b = 4)

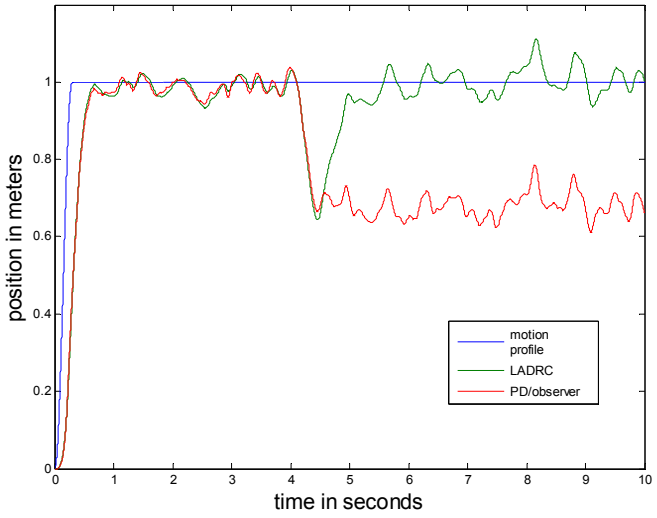

Figure 6: Performance comparison under constant force disturbance

The variation in the value of the stiffness parameter affected the PD/observer, which exhibited a noticeable steady-state error when K_b = 4 N/m. The steady-state error of the PD/ESO was not noticeably affected as compared to the case when K_b = 0.25 N/m (above the noise level) by the change. This corroborates our previous frequency response analysis of the PD/ESO, demonstrating that it has low sensitivity to variations in plant parameters. Theoretically, a conventional PD controller is not capable of rejecting a constant disturbance without steady-state error. However, Figure 6 shows that in combination with the ESO, the PD is capable of rejecting a constant-force disturbance.

VI. Simulation Results – Three Degrees of Freedom

Even though the one degree of freedom rotor system model illustrates the fundamentals of dynamics and control of a flywheel, a higher degree of freedom model is often used to describe rotor vibrations. In this section, we present a three degree of freedom model based on a distributed three-mass point system (Figure 7). The flywheel rotor-bearing system is modeled by a simply supported flexible beam, which consists of three mass points, each of which is free to move up or down in one dimension. This model [18] is capable of describing synchronous rotor vibration, which is caused by a mass imbalance in the rotor.

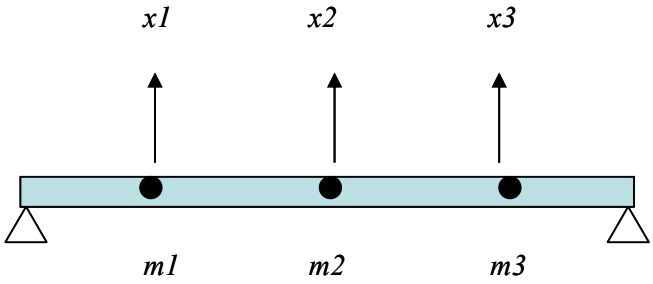

Figure 7: Simply supported beam modeled by three lumped masses

The general equation of motion for this distributed system is

$$\mathbf{M}\ddot{\mathbf{x}} + \mathbf{C}\dot{\mathbf{x}} + \mathbf{K}\mathbf{x} = \mathbf{F}(t) + \mathbf{u} + \mathbf{Q}(t) \qquad (6.1)$$

Where **M** is the mass matrix, **C** is the damping matrix and **K** is the stiffness matrix. For the system with three lumped masses, **x** is a vector of three degrees of freedom (x1, x2, x3), which gives the vertical displacement of the three masses in Figure 7. The terms on the right hand side of equation (6.1) are the rotor imbalance force **F**(t) and the control input **u**. An external force **Q**(t) may be included, which models the imbalance torque caused by the motor. The mass and damping matrix contain only diagonal elements. The cross-damping terms are negligible. The rotor imbalance forces are sinusoidal, and are of the form $f_1 = m_1 \cdot e_1 \cdot (\ddot{\phi}\sin\phi + \dot{\phi}^2\cos\phi)$ where e_1 is the eccentricity of the first mass point, and ϕ is the angular position of the rotor, and $\dot{\phi} = w$ is the rotation speed. The equation of motion thus becomes nonlinear and time-varying

In the following simulation, the rotor is to reach an operating speed of w = 300 rad/s in 0.5 second, starting from zero initial speed. The following two graphs show that the vibration amplitudes associated with PD/ESO control are three to four times less than those of the PID control, confirming the superiority of PD/ESO for rotor vibration reduction. This is especially true at higher speeds. We also note that the output amplitudes of both controllers are very similar.

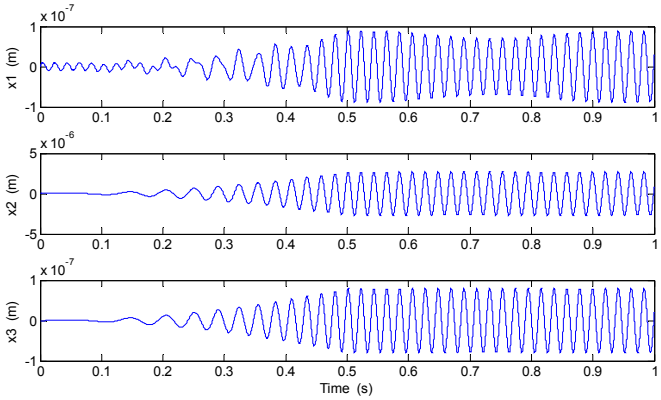

Figure 8: PID Control

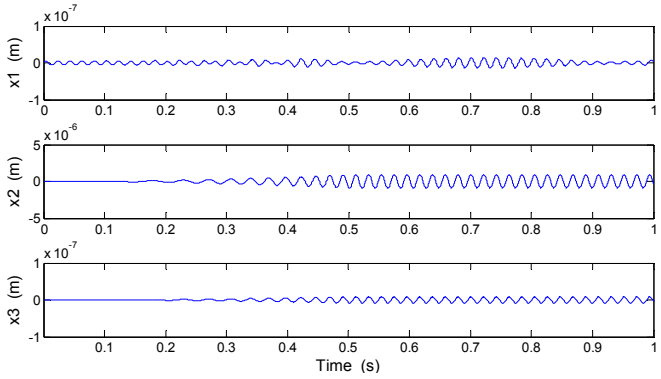

Figure 9: PD/ESO Control

VII. Conclusion

The analysis and simulation results described above demonstrate that the PD/ESO is superior to the PD observer in both disturbance rejection and robustness. In the opinion of the authors, the HSS magnetic bearing control will significantly benefit from the implementation of the PD/ESO control system, because variations in plant parameters and disturbances are always present in a real bearing system. In addition, the PD/ESO is remarkably easy to tune. The parameterization technique has even further decreased the usual number of tuning parameters and greatly facilitated the tuning of the observer. Both factors have been a concern in NASA Glenn's choice of controller design. The PD/ESO controller is also applied to a three-degree-of freedom distributed mass model and outperforms the PID in rotor vibration reduction.

The authors gratefully acknowledge Dr. Paul Lin for his expert guidance in rotor vibration control. The research is supported by grants from the NASA Glenn Research Center and Department of Energy, Assistantships from Fenn College of Engineering at Cleveland State University, as well as the Graduate College's DDREA Program.

References

[1] Schweitzer, "Active Magnetic Bearings," vdf Hochschulverlag AG, Zurich, 1994.

[2] Stienmier, "Analysis and control of a flywheel energy storage system with a hybrid magnetic bearing," *Trans. ASME* vol. 119, pp. 650-656, 1997.

[3] Kenny et al.., "Control of a High Speed Flywheel System for Energy Storage in Space Applications," *NASA internal report* (NASA/TM-2004-213356), 2004.

[4] Dever et al.., "Estimator Based Controller for High Speed Flywheel Magnetic Bearing System," *NASA internal report* (NASA/TM-2002-211795), 2002.

[5] Hubbard et al., "Feedback control systems for flywheel radial instabilities," *1980 Flywheel Technology Symposium Proceedings*, 1980, pp. 209-17.

[6] Stanway et al., "State variable feedback control of rotor bearing suspension systems." *Proceedings of the Third International Conference on Vibrations in Rotating Machinery*. University of York, 1984, C277/84.

[7] Sinha et al., "Sliding mode control of a rigid rotor via magnetic bearings." *ASME Biennial Conference on Mechanical Vibration and Noise*, Miami, Florida, September 1991.

[8] Salm et al., "Modeling and control of a flexible rotor with magnet bearings." *Proceedings of the Third International Conference on Vibrations in Rotating machinery*, 1984.

[9] Matsumura et al., "System modeling and control design of a horizontal-shaft magnetic bearing system." *IEEE Transactions on Magnetics*. Vol. 22, pp. 196-203, 1995.

[10] Hung, "Magnetic bearing control using fuzzy logic." *IEEE Transactions on Industry Applications* vol. 31, pp. 1492-97, 1996.

[11] Han, "A class of extended state observers for uncertain systems," *Control and Decision*, pp. 85-88, 1995.

[12] Gao, "Scaling and bandwidth-parameterization based controller tuning," *Proceeding of IEEE American Control Conference*, 2003.

[13] Alexander, Rarick, Dong, "Novel application of active disturbance rejection control to self-sensing magnetic bearings," *Proc. of the American Control Conference, New York City,* July 11-13, 2007.

[14] Miklosovic, Radke, Gao, "Discrete Implementation and Generalization of the Extended State Observer," *Proc. of the American Control Conference, Mineapolis, MN,* June 14-16, 2006.

[15] Miklosovic, Gao, "Dynamic Decoupling Method for Controlling High Performance Turbofan Engines," *Proc. of the 16th IFAC World Congress,* July 4-8, 2005.

[16] Radke, Miklosovic, "High Performance Tracking Control for the Practitioner," *Proc. of the American Control Conference, New York City,* July 11-13, 2007.

[17] R. Miklosovic, "A Robust Two-Degree-of-Freedom Control Design Technique and its Practical Application," *Proc. of the IEEE Industrial Application Society World Conference*, Oct. 3-7, 2004.

[18] M. James, "Vibration of Mechanical and Structural Systems," first edition, Harper&Row, Cambridge, 1989.

[19] Z. Gao, "A novel motion control design approach based on active disturbance rejection," Proceedings of the 40th IEEE CDC, Volume 5, 4-7 Dec. 2001 Page(s):4877 – 4882, vol.5.